



## METHOD ARTICLE

# REVISED Flow cell for *operando* X-ray photon-in-photon-out studies on photo-electrochemical thin film devices [version 2; peer review: 2 approved]

Philipp Jäker<sup>1,2</sup>, Dino Aegerter<sup>1</sup>, Till Kyburz<sup>1</sup>, Roman Städler<sup>1</sup>, Rea Fonjallaz<sup>1</sup>, Blanka Detlefs<sup>3</sup>, Dorota Koziej<sup>1,2</sup>

<sup>1</sup>Department of Materials, Laboratory for Multifunctional Materials, ETH Zürich, Zurich, Vladimir-Prelog-Weg 5, 8093, Switzerland

<sup>2</sup>Institutes of Nanostructure and Solid State Physics, Center for Hybrid Nanostructures, University of Hamburg, Hamburg, Luruper Chaussee 149, 22607, Germany

<sup>3</sup>European Synchrotron Radiation Facility, Grenoble, 71 avenue des Martyrs, CS 40220, 38043, France

**v2** First published: 07 Jun 2022, 2:74  
<https://doi.org/10.12688/openreseurope.14433.1>  
 Latest published: 23 Dec 2022, 2:74  
<https://doi.org/10.12688/openreseurope.14433.2>

## Abstract

**Background:** Photo-electro-chemical (PEC) water splitting represents a promising technology towards an artificial photosynthetic device but many fundamental electronic processes, which govern long-term stability and energetics, are not yet fully understood. X-ray absorption spectroscopy (XAS), and particularly its high energy resolution fluorescence-detected (HERFD) mode, emerges as a powerful tool to study photo-excited charge carrier behavior under operating conditions. The established thin film device architecture of PEC cells provides a well-defined measurement geometry, but it puts many constraints on conducting *operando* XAS experiments. It remains a challenge to establish a standardized thin film exchange procedure and concurrently record high-quality photoelectrochemical and X-ray absorption spectroscopy data that is unperturbed by bubble formation. Here we address and overcome these instrumental limitations for photoelectrochemical *operando* HERFD-XAS.


**Methods:** We constructed a novel *operando* photo-electro-chemical cell by computer numerical control milling, guided by the materials' X-ray and visible light absorption properties to optimize signal detection. To test the cell's functionality, semiconducting thin film photoelectrodes have been fabricated *via* solution deposition and their photoelectrochemical responses under simulated solar light were studied using a commercial potentiostat in a three-electrode configuration during HERFD-XAS experiments at a synchrotron.


**Results:** We demonstrate the cell's capabilities to measure and control potentiostatically and in open-circuit, to detect X-ray signals unperturbed by bubbles and to fluently exchange different thin film samples by collecting high-resolution Fe K-edge spectra of hematite ( $\alpha$ -Fe<sub>2</sub>O<sub>3</sub>) and ferrite thin film (MFe<sub>2</sub>O<sub>4</sub>, M= Zn, Ni) photoelectrodes

## Open Peer Review

Approval Status  

	1	2
<b>version 2</b>		
(revision)	<a href="#">view</a>	<a href="#">view</a>
23 Dec 2022		
<b>version 1</b>		
07 Jun 2022	<a href="#">view</a>	<a href="#">view</a>

1. **Alessandro Minguzzi** , Università degli Studi di Milano, Milan, Italy

2. **Walter S. Drisdell** , Lawrence Berkeley National Laboratory, Berkeley, USA

Any reports and responses or comments on the article can be found at the end of the article.

during water oxidation.

**Conclusions:** Our cell establishes a measurement routine that will provide experimental access of photo-electro-chemical *operando* HERFD-XAS experiments to a broader scientific community, particularly due to the ease of sample exchange. We believe to enable a broad range of experiments which acquired fundamental insights will spur further photoelectrochemical research and commercialization of water splitting technologies

### Keywords

Operando, operando instrumentation, measurement cell, HERFD-XAS, X-ray absorption spectroscopy, photoelectrochemical, photoelectrochemical water splitting, thin films, metal oxides



This article is included in the [Analytical Chemistry gateway](#).



This article is included in the [Green Chemistry collection](#).

**Corresponding author:** Dorota Koziej ([dorota.koziej@uni-hamburg.de](mailto:dorota.koziej@uni-hamburg.de))

**Author roles:** **Jäker P:** Conceptualization, Data Curation, Formal Analysis, Investigation, Methodology, Project Administration, Supervision, Visualization, Writing – Original Draft Preparation, Writing – Review & Editing; **Aegerter D:** Data Curation, Investigation, Methodology, Writing – Review & Editing; **Kyburz T:** Resources; **Städler R:** Investigation, Resources; **Fonjallaz R:** Investigation, Resources; **Detlefs B:** Investigation, Project Administration, Resources, Writing – Review & Editing; **Koziej D:** Conceptualization, Funding Acquisition, Investigation, Project Administration, Supervision, Writing – Original Draft Preparation, Writing – Review & Editing

**Competing interests:** No competing interests were disclosed.

**Grant information:** This project has received funding from the European Union's Horizon 2020 research and innovation programme under the Marie Skłodowska-Curie grant agreement No 641861.

*The funders had no role in study design, data collection and analysis, decision to publish, or preparation of the manuscript.*

**Copyright:** © 2022 Jäker P *et al.* This is an open access article distributed under the terms of the [Creative Commons Attribution License](#), which permits unrestricted use, distribution, and reproduction in any medium, provided the original work is properly cited.

**How to cite this article:** Jäker P, Aegerter D, Kyburz T *et al.* **Flow cell for *operando* X-ray photon-in-photon-out studies on photo-electrochemical thin film devices [version 2; peer review: 2 approved]** Open Research Europe 2022, 2:74 <https://doi.org/10.12688/openreseurope.14433.2>

**First published:** 07 Jun 2022, 2:74 <https://doi.org/10.12688/openreseurope.14433.1>

**REVISED Amendments from Version 1**

Major changes in the updated article version are:

- Claims about low electrochemical noise mentioned in the introduction have been removed.
- The section "*Operando* cell design and assembly" contains a short explanation why two instead of one  $\text{Si}_3\text{N}_4$  window have been used.
- The section "data quality under operando conditions" has been modified to include Walter Drisdell's criticism and to more clearly point out the mismatch between incoming X-ray beam and spectrometer focus to be responsible for reduced signal quality. Figure 5 has been slightly modified
- A more balanced discussion of the ionic current detection capability including a new reference has been written. Figure 6 has been slightly modified.

**Any further responses from the reviewers can be found at the end of the article**

## Plain language summary

We are confronted with the profound societal challenge to completely decarbonize our energy infrastructure. More than the eventual depletion of fossil fuels it is due to the imminent danger of climate change. To stop greenhouse gas emissions, mainly carbon dioxide, means either to establish a closed-loop carbon cycle or to end producing  $\text{CO}_2$  at all. However, recapturing previously released  $\text{CO}_2$  is the least economically and technologically feasible approach. Thus, stopping  $\text{CO}_2$  emissions practically requires to transition from thermal power plants and combustion engines to wind and solar power as well as electric engines. But fossil fuels are extremely dense energy carriers and cannot be always replaced by batteries. For stationary energy storage over long periods and for long range energy extensive transportation such as planes and ships other chemical fuels such as hydrogen will be needed. One approach to generate  $\text{H}_2$  is *via* photoelectrochemical (PEC) water splitting which basically combines a solar cell that converts sunlight into electricity and an electrolyzer that further converts electricity into chemical energy within a single device. Scientists develop new *operando* measurement techniques for real-time monitoring under real world conditions to bridge the divide between controlled laboratory conditions and complex real world environments. We designed a new measurement cell that allows to look into photoelectrochemical processes using X-ray spectroscopic techniques. We overcame the challenge to accommodate all features necessary to enable smooth photoelectrochemical operation and to extract new information from X-ray measurements. Moreover, we created a very user friendly cell where sample exchange is easy and fast. We believe this will greatly increase adoption of *operando* X-ray based techniques to study photoelectrochemical water splitting, provide valuable insights to optimize this technology and contribute to solving an important societal issue.

## Introduction

Photo- and electrochemical thin film devices are ubiquitous in current energy conversion technologies such as solar cells or electrolyzer. Their principal geometry enables precise control

and determination of surface area, thickness and optical path lengths, which are fundamental to determine related physical properties of materials like the absorption coefficient, conductivity and device performance metrics such as current density. Photo-electro-chemical (PEC) water splitting represents a promising thin film based application integrating photovoltaic and electrosynthetic functions within a single device to produce hydrogen as energy storage medium<sup>1,2</sup>. Overarching research goals on the path towards commercialization are the realization of conversion efficiencies competitive with solar thermal water splitting or wind and solar power driven electrolyzers and long term device stability ( $\sim 10 - 20$  years)<sup>3-5</sup>. Due to the topical complexity, a common research strategy relies on explorative and iterative materials engineering<sup>6-8</sup>. We observe continuously raising energy conversion efficiencies, but underlying photoelectrochemical processes still remain unexplored and thus we are lacking a more fundamental understanding of this technology<sup>9</sup>.

In PEC devices, semiconductor liquid electrolyte interfaces are modelled analogous to Mott-Schottky contacts, for which physical parameters are not assumed to be modified during operation<sup>10</sup>. However, based on recent results for  $\text{BiVO}_4$ , an n-type semiconductor photoanode, photocorrosive processes alter the material's chemical and morphological state during operation<sup>11,12</sup>. X-ray absorption spectroscopy (XAS) is particularly appealing to study materials and devices under working conditions due to its high penetration depth and chemical selectivity<sup>13,14</sup>. Moreover, in HERFD (high energy resolution fluorescence-detected)-XAS, the energy resolution is enhanced by wavelength dispersive detection of the X-ray fluorescence, giving access to subtle spectral feature variations such as observed in  $\text{CO}_2$  sensing<sup>15</sup>. *Operando* experiments provide new insights such as an electrochemically induced surface layer<sup>16</sup> or light excited charge transfer<sup>17</sup> and are becoming common to analyze electrochemical (electrocatalysis, batteries)<sup>18,19</sup> and photochemical processes<sup>20</sup>. In these areas, the fundamental physical interaction is either electrical or optical and the device only needs to provide electrical connection or light transparency but not both. Device operating constraints for purely electrochemical or photochemical *operando* cells are lowered and thus simplify the *operando* cell design. However, to study photo-electro-chemical processes both qualities have to be ensured simultaneously, increasing the complexity of the cell design.

The few existing examples of *operando* XAS photo-electrochemical studies interpret their findings as photoexcited charge transfer, either between atoms of two different materials as in the case of  $\text{Nb:SrTiO}_3/\text{MnO}_x$ <sup>21</sup> and  $\text{Fe}_2\text{O}_3/\text{IrO}_x$ <sup>22</sup> or within the same material as for  $\text{Fe}_2\text{O}_3$ <sup>23</sup>. In semiconductor photoelectrochemistry the challenge is to disentangle effects caused by the electrical bias and light absorption. Photoinduced phenomena are often studied using pump-probe techniques utilizing coherent monochromatic laser light<sup>24</sup>. However, lasers high irradiance leads to numerous excited states that are only probed in narrow spectral regions and might not be representative of the excitations induced by solar light in a broad spectral region. Here, we are interested in studying processes under realistic conditions utilizing standard PEC devices architecture under full solar

spectral illumination. To this end, the cell requires three electrodes to record electro-chemical current voltage (I-V) signals and shall be designed to minimize solar light and X-ray attenuation. Current cell versions often do not minimize X-ray beam attenuation resulting from high material thicknesses<sup>25,26</sup>. A further challenge is a complicated and irreversible sample exchange mechanism. For instance, depositing samples directly onto the cell's window material, such as  $\text{Si}_3\text{N}_4$ , transforms the costly part into a non reusable one<sup>23</sup>. We address the above mentioned shortcomings by realizing an *operando* cell that enables us to record high-quality X-ray absorption spectra and to adequately control current-voltage responses. Switching thin film materials for sequential *operando* measurements is achieved in a very straightforward manner and enables reproducible experiments on a series of samples (Figure 1).

## Methods

### Chemicals

The full list of chemicals used in this research are as follows: Acetonitrile (ACN), Sigma-Aldrich, 99.8%; Benzyl alcohol, Sigma-Aldrich, 99.8% anhydrous;  $\text{CuSO}_4$ , Sigma-Aldrich, anhydrous, powder,  $\geq 99.99\%$  trace metals basis; Ethanol ( $\text{EtOH}$ ), Sigma-Aldrich, standard for GC; Diethylether ( $\text{Et}_2\text{O}$ ), Sigma-Aldrich, Laboratory Reagent,  $\geq 99.5\%$  (GC); Isopropanol (IPA), Alfa Aesar, ACS,  $\geq 99.5\%$ ; 2- 2-(2-methoxyethoxy)ethoxy acetic acid (MEEAA), Sigma-Aldrich, technical grade; NaOH, Sigma-Aldrich, reagent grade,  $\geq 98\%$ , pellets (anhydrous);  $\text{NH}_4\text{OH}$ , Sigma-Aldrich, puriss. p.a., reagent ISO, reagent Ph. Eur.,  $\sim 25\%$   $\text{NH}_3$  basis;  $\text{Fe}(\text{acac})_3$ , Sigma-Aldrich, 97%;  $\text{Zn}(\text{OAc})_2$ , Sigma-Aldrich, 99.99% trace metal basis;  $\text{Ni}(\text{OAc})_2 \times 4 \text{H}_2\text{O}$ , Sigma-Aldrich, 99.99% trace metal basis. All chemicals were used without further purification.

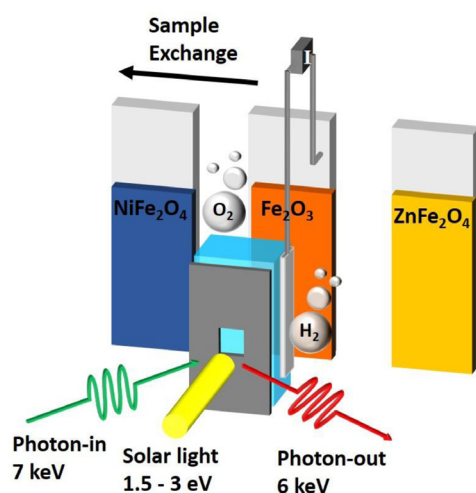


**Figure 1.** Illustrating the key *operando* cell characteristics of a fast thin film sample exchange, concurrent X-ray excitation (green) and solar excitation (yellow) while measuring the X-ray fluorescence (red) and electrochemical (grey electrodes and wires) response.

### Nanoparticle synthesis

Ferrite oxide nanoparticles ( $M\text{Fe}_2\text{O}_4$ ,  $M = \text{Zn, Ni, Fe, Co, Mn}$ ) are synthesized using a slightly modified benzyl alcohol route<sup>27,28</sup>. All particles were prepared in 10 mL benzyl alcohol poured into a 25 mL round-bottom glass flask. To obtain  $\text{ZnFe}_2\text{O}_4$  nanocrystals, 1 mmol (354 mg) of  $\text{Fe}(\text{acac})_3$  and 0.5 mmol (90 mg) of  $\text{Zn}(\text{OAc})_2$  were used as precursors.  $\text{NiFe}_2\text{O}_4$  nanoparticles (NPs) are produced from 1 mmol (354 mg) of  $\text{Fe}(\text{acac})_3$  and 0.5 mmol (125 mg) of  $\text{Ni}(\text{OAc})_2 \times 4 \text{H}_2\text{O}$ . Use of only 1 mmol (354 mg) of  $\text{Fe}(\text{acac})_3$  yield  $\text{Fe}_3\text{O}_4$  NPs that were precursors to form  $\text{Fe}_2\text{O}_3$  NPs upon calcination. All chemicals are stored inside a glovebox under Argon atmosphere. To dissolve precursors in benzyl alcohol the flask is kept at  $100^\circ\text{C}$  for two hours in an oil bath and then transferred to a preheated  $220^\circ\text{C}$  hot oil bath to avoid the formation of undesired zinc oxides phase. The flask is cooled down to room temperature (RT) and its content is completely poured into a 50 mL centrifuge tube. The flask is rinsed with few mL of  $\text{Et}_2\text{O}$  and added to the centrifuge tube. The  $\text{Et}_2\text{O}$  induces precipitation of the nanoparticles. Centrifugation for 30 min at 4000 rpm separates the nanoparticles from the liquid. The supernatant is discarded and the tube is refilled with 30 mL of a 1:1 solution of  $\text{EtOH}$  and  $\text{Et}_2\text{O}$ . The sedimented solid residue is whirled up and the tube is centrifuged again for 30 min at 4000 rpm. This process is repeated twice. The solid residue is dried at  $60^\circ\text{C}$  for two hours and finely ground.

### Photoelectrode preparation

Photoanode thin films are fabricated from preformed ferrite oxide ( $M\text{Fe}_2\text{O}_4$ ,  $M = \text{Zn, Ni, Fe, Co, Mn}$ ) nanoparticles by spin-coating on fluorine-doped tin oxide (FTO) covered glass substrates ( $1.5 \text{ cm} \times 3.5 \text{ cm}$ ,  $7 \Omega/\text{sq}$ , Solaronix). Prior to use, each FTO substrate is cleaned according to the following procedure. The substrate is consecutively placed into a solution of soap (Migros) water, absolute  $\text{EtOH}$  and deionised water while being sonicated for 15 min. Afterwards, it is immersed into an IPA solution and dried in a nitrogen stream. The spin-coating solution is prepared by dispersing 60 mg of ferrite nanoparticles in a homogeneous mixture of 940  $\mu\text{L}$  ACN, 40  $\mu\text{L}$  deionised water and 20  $\mu\text{L}$  MEEAA which functions as stabilizer<sup>28-30</sup>. After sonicating for 30 min larger agglomerates are removed by filtration to increase the dispersion's (ink) stability with a Chromafil Xtra PTFE-45/25 Syringe Filter from Macherey-Nagel of 450 nm in pore size. Next, 60  $\mu\text{L}$  ink is spin-coated onto FTO for thin film preparation. We employ a WS-650-23NPP Spin Coater from Laurell Technologies to spin the substrate for 30 s at 4000 rpm in nitrogen atmosphere. Immediately after spin-coating the substrates are dried at  $300^\circ\text{C}$  for 10 min using a pre-heated MR 3004 Safety Hotplate from Heidolph and are let to cool down to RT. Next, the substrates were covered by a ceramic bowl and are heated to  $700^\circ\text{C}$  at a rate of  $10^\circ\text{C min}^{-1}$  for 2 hours in a RHF16/3/3216P1 High-Temperature Box Furnace from Carbolite. The temperature treatment transforms  $\text{Fe}_3\text{O}_4$  into  $\text{Fe}_2\text{O}_3$  nanoparticles whereas  $\text{ZnFe}_2\text{O}_4$  and  $\text{NiFe}_2\text{O}_4$  preserve their crystalline phase. Grazing Incidence X-ray diffraction (GIXRD) confirms crystallinity and phase purity as shown in Figure S5 (see *Extended data*<sup>31</sup>). We determine film thickness from cross-sectional scanning electron microscopy



images (SEM) to about 50–80 nm exemplary shown for  $\text{ZnFe}_2\text{O}_4$  in Figure S3 (see *Extended data*<sup>31</sup>).

### Grating-incidence X-ray diffraction (GIXRD)

GIXRD experiments of all thin films were conducted with a PANalytical X'Pert Pro producing  $\text{Cu-K}\alpha_{1,2}$  radiation that is parallelized using a parabolic W/Si X-ray mirror. The incident beam size is reduced by a  $1/32^\circ$  slit and its intensity is lowered using a 0.125 mm thick Ni-based programmable beam attenuator. The reflected beam passes a  $0.18^\circ$  parallel plate collimator and is detected on a Xe-proportionality detector. First, an X-ray reflectivity scan in Omega-2Theta geometry was performed to determine the critical angle of total reflection. Afterwards, a slightly higher fixed incident beam angle at around  $0.7^\circ$  was chosen for GIXRD measurements in 2theta geometry. Raw data and the explicit data treatment (normalization and vertical translation) using *OriginPro 2017* b9.4.0.220 are accessible from *Underlying data*<sup>31</sup>. Freely available software alternatives for data treatment and plotting are *SciDavis* or *LabPlot*.

### Scanning electron microscopy (SEM)

SEM cross-sectional images were taken on a Zeiss Leo 1530 equipped with an in-lens detector. Electrons were accelerated with 3 kV and the beam was scanned across the thin film at a working distance of 4.8 mm. *ImageJ*<sup>32,33</sup> was used to enhance contrast and brightness of the whole image and to crop out the relevant section.

### Photographs

Optical images of the *operando* cell and the thin films were taken with a Panasonic DMC FZ200 under variable magnification and exposure time. *ImageJ* 1.51j8 was used to enhance contrast and brightness of the whole image and to crop out the relevant section.

### Crystal structure visualization

The *VESTA* 3.4.0 program<sup>34</sup> was used to visualize the crystal structures. Crystallographic Information Files (CIFs) of  $\text{Fe}_2\text{O}_3$ <sup>35</sup> (ICSD collection code 40142) and  $\text{ZnFe}_2\text{O}_4$ <sup>36</sup> (ICSD collection code 75097) were obtained from the *Inorganic Crystal Structure Database (ICSD)*. The *Open Crystallography Database (COD)* provides an alternative free access to crystallographic information files.

### Photoelectrochemical experiments

We produced a pH 13.6 solution by preparing a 1 mol  $\text{L}^{-1}$  sodium hydroxide electrolyte. The stock solution was prepared by adding 40 g of NaOH to 1 L Milli-Q® water (18.2  $\text{M}\Omega\cdot\text{cm}$ ). The electrolyte is pumped through the cell with an average flow rate of 1  $\text{mL min}^{-1}$  using a Harvard Apparatus PHD ULTRA Syringe Pump. We use 50 mL plastic syringes and cannulas, 0.8 mm in diameter that are squeezed into PTFE tubes of 0.7 mm in diameter. The tubes are connected to the *operando* cell using flangeless tube end fittings (Vici) that are screwed into M5 threads.

The electrochemical cell hosts three electrodes in which the FTO substrate serves as working electrode (WE), a Pt-wire

acts as counter electrode (CE) and a Radiometer REF321 (Ag/AgCl/KCl 3 M) is the reference electrode (RE). The Pt-wire has 0.5 mm  $\varnothing$ , with a  $\sim 7.3$  mm long electrolyte immersed segment providing 1.4  $\text{mm}^2$  or 0.014  $\text{cm}^2$  electrolyte exposed geometrical surface area. The reference potential of 212 mV vs standard hydrogen electrode (SHE) was converted onto the RHE (reversible hydrogen electrode) scale using the Nernst equation. The three electrodes are electrically connected using clamps. The current-voltage (I-V) experiments were realized using either a BioLogic VMP3 or a portable BioLogic SP-150 potentiostats. A potential range of -2.5 to +2.5 V is chosen, resulting in a 100  $\mu\text{V}$  resolution. A fixed current range of 1 mA and a bandwidth factor of 5 is selected. The current average over 0.1 s is recorded. Solar-like irradiation was provided either by an Oriel solar simulator equipped with a 300 W Xe lamp which light emission was spectrally adjusted to resemble an AM 1.5 G spectrum using a dedicated filter or by a Lumixo-S plasma lamp (Lumartix) providing illumination closely resembling the AM 1.5G spectrum without need for spectral adjustment. Light intensity stemming from the Oriel solar simulator was further reduced with a neutral density filter (Newport, FS-ND). For both light sources, final intensity calibration was achieved by placing the PEC cell at a distance that provided a power density of 100  $\text{mW/cm}^2$  previously determined using a calibrated Si-photovoltaic reference cell (Oriel, 91150V). The illuminated surface area on the photoelectrode was 0.280  $\text{cm}^2$  and 0.031  $\text{cm}^2$  for in-house and *operando* cell, respectively. For *operando* experiments an optical fibre was used to direct the light from the solar simulator onto the photoelectrode. We thoroughly rinsed all components in contact with the sodium hydroxide solution (electrodes, cell interior,  $\text{Si/Si}_3\text{N}_4$ -chip) with deionized water after each use. Raw data and the explicit data treatment using OriginLab Pro are available in *Underlying data*<sup>31</sup>.

### Operando cell

Technical drawings were created using the *Autodesk Inventor* 2017 software. *FreeCAD* is a freely available software alternative to view the 3D CAD files. The cell is machined from poly(methylmethacrylate) (PMMA) and additionally equipped with  $\text{Si}_3\text{N}_4$  windows. To this end, the two  $\text{Si}_3\text{N}_4$  membranes (1.2 mm (width)  $\times$  1.3 mm (length)  $\times$  500 nm (height)) are embedded into a 15 mm  $\times$  15 mm Si-chip (Norcada Inc). The technical drawings are provided as CAD files in *Underlying data*<sup>31</sup>. The CAD files are provided as .ipt & .stp (identical to .step). The latter can be imported using FreeCAD.

### HERFD-XAS

Experiments were carried out at ID26 at the European Synchrotron Research Facility (ESRF) in Grenoble, France. To obtain Fe K-edge X-ray absorption spectra the incident beam was monochromatized using a double crystal monochromator with Si (111) crystals and tuned around the absorption edges of Fe and Ni, at 7112 eV and 8333 eV, respectively. The X-ray fluorescence was detected using a wavelength-dispersive Johann-type spectrometer in Rowland geometry which operated with five spherically bent Ge (440), Ge (620) or Si (620) crystals, to selectively reflect and focus Fe  $\text{K}\alpha_1$ -,  $\text{K}\beta_{1,3}$ - or Ni  $\text{K}\alpha_1$  radiation onto an avalanche photodiode (APD) detector. The total energy resolution given as the full width at half maximum

(FWHM) of the elastic peak was 1.3 eV for Fe  $K\alpha_1$ , 1.4 eV for Fe  $K\beta_{1,3}$  and 1.6 eV for Ni  $K\alpha_1$ . A typical HERFD-XAS scan was measured from 7100 eV to 7200 eV for the Fe K-edge and from 8325 eV to 8414 eV for the Ni K-edge with a step size of 0.1 eV and a duration of 60 s per scan. All scans were corrected for the APD dead time and were normalized with respect to the beam intensity and total spectral area (TSA), being determined *via* the trapezoid rule, using PyMca 5.5.4 and OriginLab Pro, unless noted otherwise. Raw data and the explicit data treatment using PyMca and OriginLab Pro are available in *Underlying data*<sup>31</sup>. To improve the signal-to-noise ratio (SNR) in *operando* experiments we averaged over 30 scans.

## Results and discussion

### *Operando* cell design and assembly

The underlying idea was to conceive a measurement cell that provides consistent instrumental conditions, such as electrical connection and optical path length to explore, in a reproducible way, aqueous photo- and electrochemical processes occurring in thin film materials. The cell is dedicated for the use of conductive substrates such as fluorine-doped tin oxide (FTO) or indium tin oxide (ITO). It consists of six main parts which are front, back, fastening and transducer as well as Si/Si<sub>3</sub>N<sub>4</sub>-chip and photoelectrode as shown in Figure 2 a–b. The front part accommodates in- and out-flow connections, electrode slots, a mold to insert the photoelectrode and the Si/Si<sub>3</sub>N<sub>4</sub> chip as well as the

aperture. The front part is joined with the back part, which contains a threaded fastening. The transducer transfers the exerted pressure and reduces shear forces onto the photoelectrode and Si/Si<sub>3</sub>N<sub>4</sub> chip. This architecture employs only mechanical forces for sealing and hence allows a rapid sample exchange. This decisive feature decouples sample preparation, i.e. the applied thin film deposition technique, from cell assembly and allows to probe thin films fabricated from physical and chemical methods. Additionally, the straightforward mechanical photoelectrode insertion reduces the necessarily needed and often costly Si/Si<sub>3</sub>N<sub>4</sub> chip to a single and reusable quantity. This is significantly more practical and inexpensive opposed to approaches where the sample is directly deposited onto the Si<sub>3</sub>N<sub>4</sub> membranes<sup>23</sup>. The sealing between the thin film and Si-chip is realized by compression and therefore it has to be ensured that films have even surfaces. The cell is designed to operate in a typical three electrode configuration, in which the photoelectrode acts as the working electrode (WE) and its operating voltage is measured against a reference electrode (RE). A commercially available Ag/AgCl electrode is chosen as RE which is encapsulated by a glass body that is inserted into the cell's RE-slot and sealed with a pair of O rings as shown in Figure 2 b. The counter electrode (CE), a Pt-wire, compensates the current generated at the WE and is tightened by a rubber conus and a teflon tape. Principally, the RE and CE can be exchanged for measurements in electrolytes of different

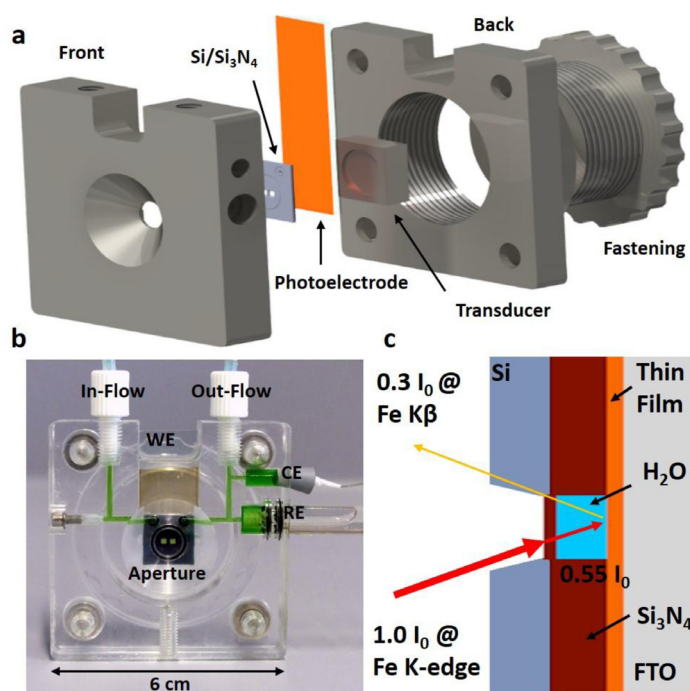


**Figure 2.** The schematics of the cell used for *operando* hard X-ray photon-in photon-out spectroscopy studies under photo-electro-chemical water splitting conditions. (a) The exploded view highlights the most important components such as the front, transducer, back and fastening parts (dark grey), Si/Si<sub>3</sub>N<sub>4</sub> chip as optical aperture for UV-Vis and X-ray beam (light grey) and photoelectrode (orange). (b) Photograph of the cell showing the three electrodes configuration: thin-film based photoelectrode as WE, platinum wire as CE and Ag/AgCl electrode as RE. A green-colored solution is used to visualize the electrolyte path inside the cell. (c) A schematic illustrating the optical path in a photon-in-photon-out process. The X-ray intensities incident on the sample and on the detector are given after passing 500 nm of Si<sub>3</sub>N<sub>4</sub> and 400  $\mu$ m of water for the Fe K-edge upon absorption (photon-in at 7112 eV) and for the Fe  $K\beta_{1,3}$  line upon emission (photon-out at 7059 eV).

pH-values or for anodically more active electrodes, respectively. The cell's front and back parts (dark grey) shown in Figure 2 a are manufactured by computer numerical control milling from poly(methylmethacrylat) (PMMA). PMMA provides the necessary water resistivity to perform aqueous photoelectrochemical experiments and transparency, which allows to spot possible electrolyte leakage and to follow the wetting behavior of the three electrodes. Especially the RE requires uniform electrolyte coverage of the porous frit, undisturbed by gas bubbles, to ensure a stable reference potential. Electrolyte is supplied from syringe pumps *via* chemically resistant poly(tetrafluorethylene) (PTFE) tubings. They are connected to the cell's flow system *via* flangeless tube end fittings that ensure reliable, leakage-free operation. The cell's channels have a diameter of 500  $\mu\text{m}$  and are sufficiently wide for flow rates up to 5  $\text{mL min}^{-1}$ . A flow cell is advantageous to a static one as a constant temperature is maintained during solar and X-ray beam irradiation reducing possible radiation damage. Additionally, continuously refreshing the electrolyte, which is consumed during water splitting, ensures a stable pH and moreover, releases the gaseous endproducts,  $\text{H}_2$  and  $\text{O}_2$ . For mechanical stability and precise positioning, a M5 thread is implemented into the cell's front part to mount the cell onto the beamline's sample stage. The CAD files are provided in *Underlying data*<sup>31</sup>.

Central in photon-in-photon-out spectroscopy is to minimize absorption losses for both the incident and fluorescent X-rays as schematically shown in Figure 2 c. Consequently, a very thin optical window material that consists of low atomic number (Z) elements is required which is also transparent in the visible region. Thus, we employed two 500 nm thin  $\text{Si}_3\text{N}_4$  membranes as a windows, which are thick enough to provide the necessary mechanical stability to withstand the water pressure. We decided against a larger single  $\text{Si}_3\text{N}_4$  window as it would have been more brittle and thus susceptible to breaking due to the water pressure. They are embedded into a 400  $\mu\text{m}$  thick Si chip which contains a fluidic channel that connects the fluid ports to the central 2-window area. The fluidic channels are defined by a 400  $\mu\text{m}$  deep spacer, integral to the chip structure. The spacer layer is made of a multilayer of Si and  $\text{SiN}_x$  films. Although an even thinner electrolyte layer would minimize absorption effects, it might also introduce electrochemical mass transfer and flow rate limitations. Taking transmission losses into account<sup>37</sup>, we estimated that this setup retains 30 % of the original intensity (Figure 2 c) on detecting Fe K  $\beta$  fluorescence (7059 eV) while exciting at the Fe K-edge (7112 eV), as shown in detail in Section 1 of the SI and visualized in Figure S1 (see *Extended data*<sup>31</sup>). The OriginLab project file used to plot the tabulated values is provided in *Underlying data*<sup>31</sup>.

### Metal oxide photoelectrodes

We select hematite and transition metal ferrites photoelectrodes for the applicability tests of an *operando* HERFD-XAS cell. We choose hematite, because it is one of the most characterized metal oxide photoanode for water oxidation and served as model compound for *in situ* XAS and XPS studies<sup>23,38</sup>. Transition metal ferrites of the composition  $\text{MFe}_2\text{O}_4$  ( $M = \text{Mn, Co, Ni \& Zn}$ ) are ternary oxides that offer to tune the optoelectronic properties by varying the non-iron cation<sup>39</sup>. Similar to hematite, they have shown chemical stability for hours of operation<sup>40</sup> and are promising photoelectrochemical materials with an optical

band-gap range between 1.5 eV and 1.9 eV, that enable theoretical, assuming 100% incident-photon-to-current (IPCE) conversion, current densities from 29  $\text{mA cm}^{-2}$  to 18  $\text{mA cm}^{-2}$ <sup>241</sup>. Among the transition metal ferrites nanoparticles that are accessible *via* the benzyl alcohol route<sup>27,28</sup>  $\text{MnFe}_2\text{O}_4$  and  $\text{CoFe}_2\text{O}_4$  demonstrated only marginal photocurrents and thus we exclusively focus on  $\text{ZnFe}_2\text{O}_4$  and  $\text{NiFe}_2\text{O}_4$  with  $\text{Fe}_2\text{O}_3$  as the model photoelectrodes for *operando* HERFD-XAS studies, see Figure S2 (*Extended data*<sup>31</sup>). for corresponding photocurrent measurements. Additional information on crystal structure and thin film morphology including its thickness can be found in *Extended data*<sup>31</sup>, section 2 Figure S3–S6.

### Photoelectrochemical measurements

Inferring mechanistic information from X-ray spectral changes relies on the controllable and predictable behavior of the applied stimulus i.e. electrical potential and solar illumination and their measurable effect. Thus, we compare the *operando* cell to a commonly used standard laboratory photoelectrochemical cell<sup>42</sup>. Conducting photoelectrochemical experiments on the same material but in two different cells should reveal apparatus-related differences. Our analysis focuses on the working electrode potential regulation and photocurrent measurements.

Therefore, we compared constant potential or chronoamperometric measurements of  $\text{Fe}_2\text{O}_3$  photoanodes in our *operando* cell with 0.031  $\text{cm}^2$  illuminated area versus our laboratory cell with 0.28  $\text{cm}^2$  illuminated area as shown in Figure 3. The measurement protocol includes a stepwise potential increase after 360 s during which dark and illuminated periods alternate

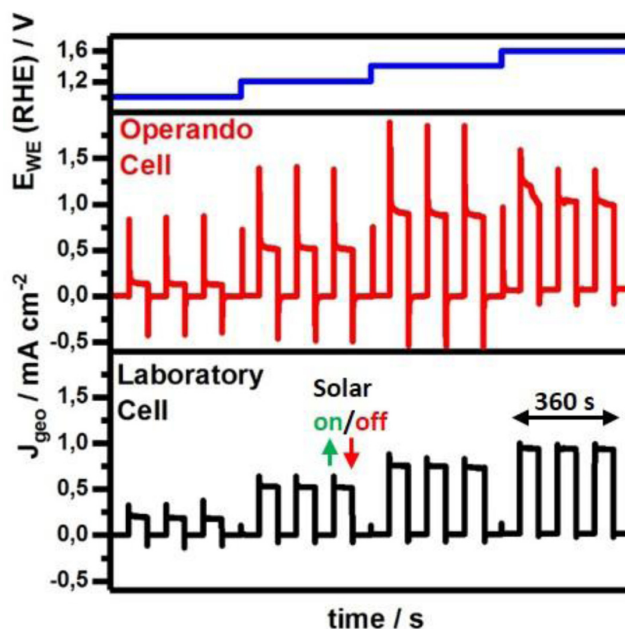


**Figure 3.** Comparison of photocurrent densities of the  $\text{Fe}_2\text{O}_3$  photoanodes under constantly applied potentials (blue) recorded in the *operando* flow cell (red) and laboratory cell (black). Photocurrent measurements show that the *operando* cell generates low noise, and the photocurrent densities  $J_{\text{geo}}$ , normalized to the geometrically illuminated area, are similar to those obtained in the laboratory cell.



every 60 s. The applied potential follows the set potential from 1.0 to 1.6 V vs RHE in steps of 0.2 V and demonstrates the successful voltage regulation (Figure 3, top). In the dark, recorded current densities are  $0.001\text{--}0.005\text{ mA cm}^{-2}$  for both cells in the applied potential range of 1.0 V to 1.4 V indicating no significant faradaic processes. At 1.6 V the applied potential starts to match the kinetic overpotential causing water oxidation with a rate up to  $0.07\text{ mA cm}^{-2}$  in the *operando* cell, which is about  $0.05\text{ mA cm}^{-2}$  ( $\sim 3.5$  times) greater than for the laboratory cell with  $0.02\text{ mA cm}^{-2}$ . However, contrary to the laboratory cell which provides equally sized dark and illuminated areas on the photoelectrode, the *operando* cell's total electrolyte exposed geometric surface area towards the photoelectrode amounts to  $0.172\text{ cm}^2$  (Figure S7 in *Extended data*<sup>31</sup>) and is about 5.5 times larger than the illuminated area. Therefore, renormalization corresponding to a current density reduction by a factor of 5.5 to  $0.013\text{ mA cm}^{-2}$  reveals current densities in the laboratory cell to be 1.6 times higher. During illumination and under potentials of 1.0 V vs RHE values stabilize at  $0.25\text{ mA cm}^{-2}$  and are doubled to  $0.5\text{ mA cm}^{-2}$  upon potential increase to 1.2 V. Within this voltage window the photocurrent densities recorded in our *operando* cell match very well the values obtained in the laboratory cell. However, by increasing the applied potential further to 1.4 V and 1.6 V the *operando* cell delivers slightly higher steady-state photocurrent densities of about  $0.90\text{ mA cm}^{-2}$  and  $1.05\text{ mA cm}^{-2}$ , respectively than the laboratory cell with  $0.75\text{ mA cm}^{-2}$  and  $0.95\text{ mA cm}^{-2}$ , respectively. Whether in the dark or under illumination, recorded current densities deviate at higher applied voltages for which the effect of potentially different solution resistances would be amplified. Further contributing factors are related to variations during sample preparation<sup>43</sup> or potential sample modification under operation<sup>44,45</sup>, both itself promising research topics but difficult aspects to control due to the material's physical complexity. However, electrolyte mass transfer behavior will clearly be affected as the cell's geometry is modified and liquid flow is actively driven compared to the static laboratory cell. Up to now, we considered steady-state values varying maximally about 1.6 times but observe 7–8 times variation in transient peak current densities upon triggering solar illumination or a potential step (Figure S8 in *Extended data*<sup>31</sup>). Such transients are common in chronoamperometric experiments in the dark<sup>46</sup> and under illumination<sup>47,48</sup> and are explained *via* non faradaic charging processes, both within the semiconductor and electrolyte, or *via* electrolyte diffusion after initial near-electrode depletion. As the same transient behavior is observed for measurements on a different material, namely  $\text{NiFe}_2\text{O}_4$  (Figure S9 in *Extended data*<sup>31</sup>), the underlying cause might be cell geometry and flow.

The previous discussion is a starting point to understand the *operando* cell's photoelectrochemical characteristics. In future, more quantitative work will rely on comprehending its current-voltage behavior in detail particularly regarding uncompensated solution resistance lowering the electrical potential the WE actually experiences. However, the near steady state conditions are reached within seconds after the external stimulus (light or bias) and can be reproduced multiple times for

extended periods (Figure 6) allowing repeatable XAS scans to be averaged, as discussed in the next section. Therefore, we conclude that photoelectrochemical conditions are maintained that closely resemble laboratory testing conditions and allow to qualitatively investigate associated phenomena of thin film photoelectrodes using X-ray absorption spectroscopy.

In addition, the operation in continuous flow provides significant advantages. We maintain a constant temperature and thus can exclude thermally induced effects due to UV-Vis and X-ray absorption as opposed to photo-electro-chemical effects. In the same instance, we avoid the formation of gaseous bubbles that can adsorb onto the photo-electrodes surface and decrease the active surface area, which would lower the photocurrent. Additionally, as gas droplets are of lower density than water, they enhance transmission of both UV-Vis light and X-rays. Frequent density variations along the X-ray beam path lead to abrupt, spike like intensity fluctuations and generate unreliable data that cannot be normalized for. Consequently, by minimizing gas accumulation our *operando* cell raises the amount of high-quality valid data.

#### Data quality under *operando* conditions

Assuming the energy resolution is unaffected by measuring under *operando* conditions, the signal-to-noise ratio (SNR) is an important parameter characterizing the data quality. Here, the SNR is described as quotient of the arithmetic mean  $\mu$  and the standard deviation  $\sigma$ <sup>49,50</sup> and is proportional to the square root of the signal obtained under identical conditions<sup>51</sup> either *via* prolonged measurement or *via* averaging of consecutive measurements<sup>52</sup>. We assume non-correlated measurements with time invariant white noise to be present in the measured spectral range<sup>53</sup>. To calculate the SNR the spectral region from 7180 eV to 7184 eV was chosen, in which the measured intensity was almost constant. To assess the additional time required to compensate for absorption losses caused by the electrolyte and the  $\text{Si}_3\text{N}_4$  windows, we estimated a relative signal detection yield of 30% upon Fe K-edge absorption and K $\beta$ -fluorescence (Figure 2 c, *Extended data*<sup>31</sup> Section 1 and Figure S1), which corresponds to a SNR decrease by a factor of 1.8.

We compare two Fe K-edge scans on an approximately 50–80 nm thin  $\text{Fe}_2\text{O}_3$  film under *ex-situ* (Figure 4, left black) and *operando* conditions (Figure 4, left red). The intensity of the Fe K-edge spectrum measured in *operando* is attenuated by a factor of 11.68, representative of a detection yield of 8.56%.

To explain the deviation between estimation and experiment we need to consider the beam's spatial profile and the measurement geometry (Figure 5 a). The intensity loss is a result of the orthogonality between the photon-in beam and the mutual focus area of all 5 analyzer crystals. First, it increases the optical path length inside the electrolyte (Figure 5 b) and second it leads to a smaller area that is simultaneously covered both by the photon-in beam and spectrometer focus (Figure 5 c). The optical path length is enlarged from 400  $\mu\text{m}$  to 566  $\mu\text{m}$  which explains a lower relative detection yield of 18.7% (Extended



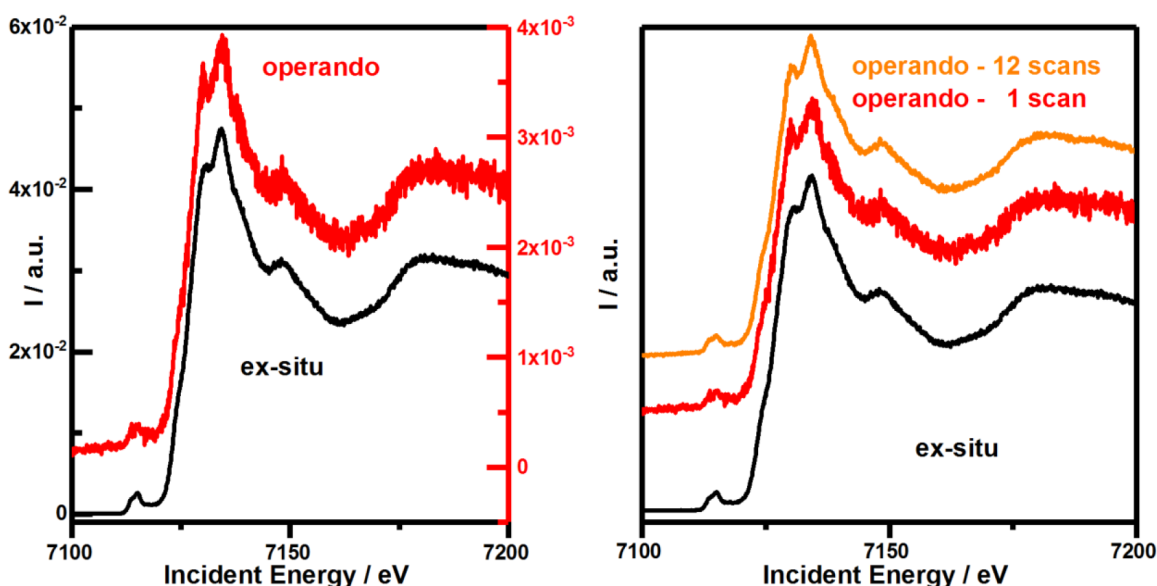


**Figure 4.** Comparing the quality of Fe K-edge spectra on  $\text{Fe}_2\text{O}_3$  obtained via  $\text{K}\beta$ -fluorescence detection under *ex situ* and *operando* conditions. The sample was measured under *ex-situ* (black) and *operando* (red & orange) conditions. Left: Single scans are recorded for 60s and normalized to incident beam intensity to compare signal intensity. Right: Scans are normalized to incident beam intensity and total spectral area (TSA) to compare the signal-to-noise ratio (SNR). Please note the different black and red scale bars corresponding to the same colored data traces in the left figure.

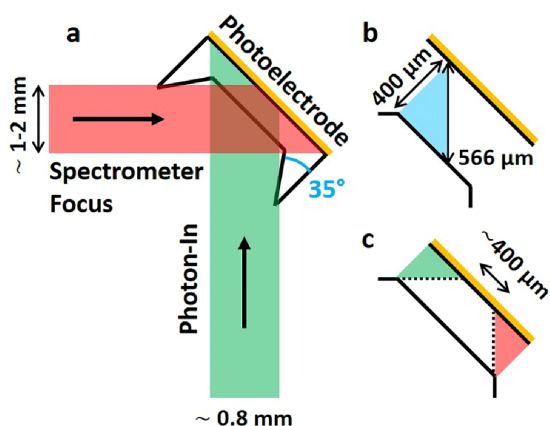


**Figure 5.** (a) Schematic (top view) illustrating photon-in (incident X-ray, green) and spectrometer focus (red) beam profiles covering different regions on the photoelectrode (orange). Intensity is collected from a photoelectrode (orange) region where photon-in beam and spectrometer focus profiles overlap. Profiles are defined through incident beam size and crystal spectrometer focus size. (b) Orthogonality between photon-in beam and spectrometer focus prolongs the optical path length in the electrolyte to 566  $\mu\text{m}$ . (c) The overlapping region of photon-in and photon-out profiles is reduced to approximately 400  $\mu\text{m}$ .

data) but not as low as 8.56%. This remaining difference can be explained considering that the photon-in beam size of 0.8 mm (w)  $\times$  0.1 mm (h) yields a greater projected beam size of 1.13 mm (w)  $\times$  0.1 mm (h) on the photoelectrode which reduces the average photon flux by 0.707. A lower photon flux only reduces the measured intensity if not all of the X-ray

excited sample area is covered by the spectrometer focus which we assume is the case. The spectrometer focus diameter of all 5 crystals ( $\sim 1\text{--}2$  mm, determined from alignment scans) is large enough to cover the full area of one  $\text{Si}_3\text{N}_4$  window (1.2 mm (width)  $\times$  1.3 mm (length)). The exact focal area projection or shape on the sample, potentially spherical, is unknown but we consider it large enough to completely encompass the incident X-ray beam along its very thin axis of 0.1 mm in height. Consequently, we only need to consider one limiting spatial dimension, the width, instead of two. Here, the orthogonal detection geometry (Figure 5 a) effectively reduces the measurable sample width from the complete coverage of  $\text{Si}_3\text{N}_4$  window area down to only a width of  $\sim 0.4$  mm (Figure 5 c). The larger the distance between the  $\text{Si}_3\text{N}_4$  window and the thin film, i.e. the larger the electrolyte thickness, the smaller will be the overlap between X-ray excited sample area and spectrometer focus. This relationship becomes visually clear comparing the red and green overlapping regions (Figure 5 a) first on  $\text{Si}_3\text{N}_4$  and then on the photoelectrode thin film. 0.4 mm only represents 35.4% of the on sample projected beam size of 1.13 mm and equals the lowered detection yield. Multiplied with previously determined losses due to the extended optical path length an overall relative detection yield of 6.6% is calculated which approximates the experimentally determined 8.56% detection yield.

Thus, the SNR of a single *operando* scan compared to an *ex-situ* scan should be reduced by 3.42, square root of 11.68, but is determined to be only lowered by 3.06 (Figure 4, right and OriginLab project file in *Underlying data*<sup>31</sup>). Hence, our assumptions about non-correlated measurements and underlying white noise might not be entirely correct. An

average out of 12 *operando* scans therefore slightly exceeds the SNR of a level of an individual *ex-situ* scan (OriginLab project file in *Underlying data*<sup>31</sup>). Thus prolonged measuring or averaging consecutive measurements is effective in restoring the initially SNR of *ex-situ* measurements. Our theoretical estimation seems to capture most essential aspects that cause this decline and thus provides understanding as well as guidelines to optimize the SNR for future *operando* studies. Thus, our cell can be directly used at extremely brilliant source (EBS) storage ring like MAX IV, ESRF or after the upgrade of Petra IV at the time scales relevant for photoelectrochemical processes.

Prior to *operando* experiments, *ex-situ* HERFD-XAS measurements shown in Figure S10 (see *Extended data*<sup>31</sup>) were performed and provide no evidence for X-ray beam induced spectral changes often called “beam damage”. Finally, we conduct the *operando* experimental protocol and record HERFD-XAS spectra of hematite,  $\text{NiFe}_2\text{O}_4$  and  $\text{ZnFe}_2\text{O}_4$  (Figure S11 in *Extended data*<sup>31</sup>) under open-circuit (OC), electrochemical (EC) and photoelectrochemical (PEC) conditions. The Fe K edge excitation spectra on hematite (Figure S11 a in *Extended data*<sup>31</sup>) are recorded *via* the  $\text{K}\beta$  fluorescence line (7059 eV) and spectra on  $\text{NiFe}_2\text{O}_4$  and  $\text{ZnFe}_2\text{O}_4$  (Figure S11 b-c in *Extended data*<sup>31</sup>) are measured *via* the  $\text{K}\alpha$  fluorescence line (6405 eV) to increase the signal intensity. Note that we also recorded Ni K-edge spectra on  $\text{NiFe}_2\text{O}_4$  (Figure S11 d in *Extended data*<sup>31</sup>). Interestingly, despite high quality of the data, at minutes time scale we do not observe any changes under PEC conditions, neither in the pure HERFD-XANES spectra nor in the differential spectra ( $\Delta\text{EC}$  and  $\Delta\text{PEC}$ ) as shown in Figure S11 (see *Extended data*<sup>31</sup>). However, we want to stress that this is not a necessary premise to conclude that we nevertheless demonstrate the general applicability of our cell to measure high quality (high SNR) HERFD-XAS spectra under photoelectrochemical conditions. We provide sufficient evidence to support claims on all of the cell's capabilities. Therefore, a scientific apparatus is presented that allows to correlate independent variables (voltage, solar illumination) with dependent variables such as the material's current and X-ray emission response. This study only tested an infinitesimally small part of the available parameter space to prove the cell function's principal validity. The experimental conditions can easily be extended towards more intense or pulsed light sources and pump-probe detection schemes to study PEC effects at shorter time scales for example using time-resolved X-ray absorption spectroscopy<sup>54</sup>.

### Electrochemical X-ray absorption detection

The X-ray fluorescence (XRF) that is detected during the experiment is one of many secondary processes that follow the initial X-ray excitation. Additionally, to a radiative decay there are also non-radiative secondary processes that generate electronic or ionic currents, which can be used to measure X-ray absorption spectra. Under applied bias conditions we can distinguish the photoelectrochemical current from the periodically repeated X-ray beam induced current (Figure 6) caused by individual Fe K-edge scans. By zooming into one of the respective sections the time-dependent current profile resembles the X-ray absorption profile monitored *via* fluorescence detection (Figure 6, inset). We believe it is most plausible for these currents to be generated inside the  $\text{Fe}_2\text{O}_3$  thin film upon

Fe K-edge excitation, assuming possible Fe contamination inside the cell to be insufficient to explain these rather large current densities of about  $0.15 \text{ mA cm}^{-2}$ . It is likely that the measured current contains ionic contributions as liquid electrolyte connects working and counter electrode. Recent work attempted to clarify the current's nature, origin and potential usefulness as additional X-ray absorption measure. Early research claims that using two unbiased electrodes connected to an ammeter enables a more bulk-sensitive measure of X-ray absorption in the electrolyte while using only a single drain electrode renders the measurement sensitive to the vicinity of the electrode<sup>55,56</sup>. However, this claim has been opposed arguing that both current measurements from the one and two electrode configuration provide information sensitive to the electrodes' vicinity<sup>57</sup>. While the current's exact origin and information content are still up for debate, we believe that this opens up an exciting new research avenue in which carefully conceived electrochemical measurements will be crucial.

Instead of simply considering the current as a secondary signal that serves to record X-ray absorption spectra, it can also be applied to investigate electronic transport properties using methods that are referred to as photoconduction<sup>58</sup> or X-ray beam induced current (XBIC)<sup>59</sup> mainly in pure solid state systems. The latter technique was used to spatially map bottlenecks of low minority carrier diffusion length in multicrystalline silicon solar cells caused by metal impurities such as iron<sup>60</sup>. A short-wavelength X-ray beam can provide a much smaller illumination cross-section compared to a beam of visible-wavelength light that offers high spatial resolution and element selectivity. Both characteristics have been taken advantage of to visualize and correlate the XBIC with the elemental composition of GaAs across a single nanowire<sup>61</sup>. These examples illustrate

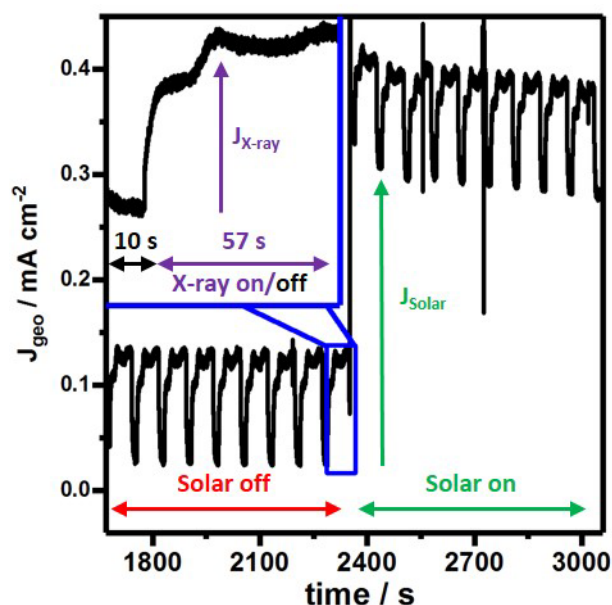


**Figure 6.** Constant potential photocurrent measurements, based on the geometrically illuminated area of  $\text{Fe}_2\text{O}_3$  photoanodes at 1.6 V vs RHE recorded in the *operando* flow cell. (Inset) During HERFD-XAS at the Fe K-edge X-ray exposure induces additional current suitable for ionic-current XAS detection or to examine charge carrier transport properties.

prospective experiments with the *operando* cell in which electrochemical current detection upon element selective X-ray excitation would allow to determine atom dependent X-ray beam induced currents such as in multinary oxides, e.g.  $\text{ZnFe}_2\text{O}_4$ , or doped semiconductors as for example Ti-doped  $\text{Fe}_2\text{O}_3$ . Thus, deeper insights into individual atomic contributions to electronic transport properties would be provided. However, this long term prospect requires a much more thorough understanding of the cell's electrochemical measurement capabilities.

## Conclusions and outlook

The *operando* X-ray absorption spectroscopy approach generally offers insight into device operation but requires a sophisticated sample environment. Studying thin films in photoelectrochemical water splitting cells poses obstacles for XAS under working conditions, as many interdependent parameters and functionalities have to be optimized. Our work approaches this challenge based on thorough estimations of radiative transmission leading to an *operando* HERFD-XAS flow cell in which the electrolyte thickness is reduced to a minimum. Consequently, the cell delivers high transparency for both visible-light (1.5–3 eV) and X-ray ( $\geq 6400$  eV) radiation. The resulting high signal-to-noise ratio enhances the detection limit and minimizes the synchrotron data collection time. Moreover, by reusing a single  $\text{Si}_3\text{N}_4/\text{Si}$  chip for multiple measurements the experimental cost is greatly reduced. PEC current and voltage can routinely be determined and controlled using a standard 3 electrode configuration connected to a commercially available potentiostat that allows to conduct numerous aqueous electrochemical experiments with low electrochemical noise. The high electrochemical and X-ray spectroscopic signal quality are prerequisite to take advantage of the cell's central aspect which is the facile thin film exchange mechanism that relies purely on mechanical fixation. Our approach treats the X-ray transparent window and thin film separately. Thus, the sample can be independently prepared and optimized. This feature made it possible to collect a comprehensive dataset on three different metal-oxide photoelectrodes during a single synchrotron beamtime (see *Underlying data*<sup>31</sup>) and can in principal be extended to any desired thin film material. Finally, we describe the potential to electrochemically measure X-ray absorption spectra that might be a suitable detection method for lower X-ray energies. Alternatively, recording the X-ray beam induced current (XBIC) that is element-specific might layout atomic contributions to photocurrents, possibly with high spatial resolution using an X-ray microprobe. Overall, this work targets the instrumental bottleneck in *operando* fluorescence-detected X-ray absorption spectroscopy by establishing a measurement routine for experiments on photo- and electrochemical thin film devices, that significantly simplifies the technique's applicability and will stimulate further research.

## Ethics and consent

Ethical approval and consent were not required.

## Data availability

### Underlying data

Zenodo: Dataset for the development of a “Flow cell for *operando* X-ray photon-in-photon-out studies on photo-electrochemical thin film devices”. <https://doi.org/10.5281/zenodo.6560384><sup>31</sup>.

This project contains the following underlying data:

- CAD\_IPT.zip (the cell's 3D technical drawing files in the specific AutoDesk Inventor format as .ipt-files for individual parts and .iam-files for the assembly).
- CAD\_STP.zip (the cell's 3D technical drawing files in the .stp or .step format “STandard for the Exchange of Product model data”. As an ISO standard it is very accessible).
- GIXRD.zip (the GIXRD raw data on the thin film materials as .xrdml, .csv and .xy files and the OriginPro project file in which data was processed and plotted.).
- HERFD.zip (the HERFD-XAS raw data on the thin film materials conducted during ex-situ and *operando* measurements as unspecified files to be opened *via* PyMca and the OriginPro project file in which data was processed and plotted.).
- PEC-duringHERFD.zip (the photoelectrochemical raw data on the thin film materials conducted during *operando* measurements as .mpr and .mpt files, the former to be opened *via* the BioLogic software and the latter by any scientific data processing software. It also contains the OriginPro project file in which data was processed and plotted.).
- PEC.zip (the photoelectrochemical raw data on the thin film materials conducted during ex-situ measurements as .mpr and .mpt files, the former to be opened *via* the BioLogic software and the latter by any scientific data processing software. It also contains the OriginPro project file in which data was processed and plotted.).
- SEM.zip (the SEM image on the thin film materials after brightness and contrast enhancement and cropping).

## Extended data

Zenodo: Dataset for the development of a “Flow cell for *operando* X-ray photon-in-photon-out studies on photo-electrochemical thin film devices”. <https://doi.org/10.5281/zenodo.6560384><sup>31</sup>.

This project contains the following extended data:

- ExtendedData.zip (additional information arranged in a word document that are directly linked to the main manuscript such as figures).

Data are available under the terms of the [Creative Commons Attribution 4.0 International license](#) (CC-BY 4.0).

## Acknowledgements

We acknowledge the European Union for a Marie Curie ITN Grant (Photo4Future, grant number 641861) funded under H2020-EU.1.3.1, ETH Zürich, and University of Hamburg for financial support and European Synchrotron Research Facility (ESRF), ID26 for the beamtime allocation (project number MA 3560). At ETH Zürich, Materials Science Department we thank Prof. M. Niederberger for access to the chemistry lab, materials characterization equipment and helpful discussions.

Prof. Andre Studart for access to the SEM, the technical workshop for machining the *operando* cell. Christoph Willa and Raphael Peltier for assistance during the beamtime. Norcada Inc for Si-embedded Si<sub>3</sub>N<sub>4</sub> windows and support in the cell design.

PJ thanks Lukas Grote and Anke Puchert (Faculty of Physics, University of Hamburg) for helpful scientific discussions, Simon D. Klob (Ludwig-Maximilians-University of Munich) for proofreading of the manuscript.

## References

- Chu S, Cui Y, Liu N: **The path towards sustainable energy.** *Nat Mater.* 2016; **16**(1): 16–22.  
[PubMed Abstract](#) | [Publisher Full Text](#)
- Sivula K, van de Krol R: **Semiconducting materials for photoelectrochemical energy conversion.** *Nat Rev Chem.* 2016; **1**: 15010.  
[Publisher Full Text](#)
- Ardo S, Fernandez Rivas D, Modestino MA, et al.: **Pathways to electrochemical solar-hydrogen technologies.** *Energy Environ Sci.* 2018; **11**(10): 2768–2783.  
[Publisher Full Text](#)
- Detz RJ, Reek JNH, van der Zwaan BCC: **The future of solar fuels: when could they become competitive?** *Energy Environ Sci.* 2018; **11**(7): 1653–1669.  
[Publisher Full Text](#)
- Shaner MR, Atwater HA, Lewis NS, et al.: **A comparative technoeconomic analysis of renewable hydrogen production using solar energy.** *Energy Environ Sci.* 2016; **9**(7): 2354–2371.  
[Publisher Full Text](#)
- Kim TW, Ping Y, Galli GA, et al.: **Simultaneous enhancements in photon absorption and charge transport of bismuth vanadate photoanodes for solar water splitting.** *Nat Commun.* 2015; **6**: 8769.  
[PubMed Abstract](#) | [Publisher Full Text](#) | [Free Full Text](#)
- Kim JH, Kim JH, Jang JW, et al.: **Awakening Solar Water-Splitting Activity of ZnFe<sub>2</sub>O<sub>4</sub> Nanorods by Hybrid Microwave Annealing.** *Adv Energy Mater.* 2015; **5**(6): 1401933.  
[Publisher Full Text](#)
- Hufnagel AG, Peters K, Müller A, et al.: **Zinc Ferrite Photoanode Nanomorphologies with Favorable Kinetics for Water-Splitting.** *Adv Funct Mater.* 2016; **26**(25): 4435–4443.  
[Publisher Full Text](#)
- The fine line between performance improvement and device practicality.** *Nat Commun.* 2018; **9**(1): 5268.  
[PubMed Abstract](#) | [Publisher Full Text](#) | [Free Full Text](#)
- Iqbal A, Bevan KH: **Simultaneously Solving the Photovoltage and Photocurrent at Semiconductor–Liquid Interfaces.** *J Phys Chem C.* 2017; **122**(1): 30–43.  
[Publisher Full Text](#)
- Toma FM, Cooper JK, Kunzelmann V, et al.: **Mechanistic insights into chemical and photochemical transformations of bismuth vanadate photoanodes.** *Nat Commun.* 2016; **7**: 12012.  
[PubMed Abstract](#) | [Publisher Full Text](#) | [Free Full Text](#)
- Zhang S, Rohloff M, Kasian O, et al.: **Dissolution of BiVO<sub>4</sub> Photoanodes Revealed by Time-Resolved Measurements under Photoelectrochemical Conditions.** *J Phys Chem C.* 2019; **123**(38): 23410–23418.  
[Publisher Full Text](#)
- Weckhuysen BM: **Operando spectroscopy: fundamental and technical aspects of spectroscopy of catalysts under working conditions.** *Phys Chem Chem Phys.* 2003; **5**(20): 1.  
[Publisher Full Text](#)
- Singh J, Lamberti C, van Bokhoven JA: **Advanced X-ray absorption and emission spectroscopy: in situ catalytic studies.** *Chem Soc Rev.* 2010; **39**(12): 4754–4766.  
[PubMed Abstract](#) | [Publisher Full Text](#)
- Hirsch O, Kvashnina KO, Luo L, et al.: **High-energy resolution X-ray absorption and emission spectroscopy reveals insight into unique selectivity of La-based nanoparticles for CO<sub>2</sub>.** *Proc Natl Acad Sci U S A.* 2015; **112**(52): 15803–15808.  
[PubMed Abstract](#) | [Publisher Full Text](#) | [Free Full Text](#)
- Bergmann A, Martinez-Moreno E, Teschner D, et al.: **Reversible amorphization and the catalytically active state of crystalline Co<sub>3</sub>O<sub>4</sub> during oxygen evolution.** *Nat Commun.* 2015; **6**: 8625.  
[PubMed Abstract](#) | [Publisher Full Text](#) | [Free Full Text](#)
- Amidani L, Naldoni A, Malvestuto M, et al.: **Probing Long-Lived Plasmonic-Generated Charges in TiO<sub>2</sub>/Au by High-Resolution X-ray Absorption Spectroscopy.** *Angew Chem Int Ed.* 2015; **54**(18): 5413–5416.  
[PubMed Abstract](#) | [Publisher Full Text](#)
- Friebe D, Louie MW, Bajdich M, et al.: **Identification of Highly Active Fe Sites in (Ni,Fe)OOH for Electrocatalytic Water Splitting.** *J Am Chem Soc.* 2015; **137**(3): 1305–1313.  
[PubMed Abstract](#) | [Publisher Full Text](#)
- Zhang Y, Pelliccione CJ, Brady AB, et al.: **Probing the Li Insertion Mechanism of ZnFe<sub>2</sub>O<sub>4</sub> in Li-Ion Batteries: A Combined X-Ray Diffraction, Extended X-Ray Absorption Fine Structure, and Density Functional Theory Study.** *Chem Mater.* 2017; **29**(10): 4282–4292.  
[Publisher Full Text](#)
- Pfeffer MG, Schafer B, Smolentsev G, et al.: **Palladium versus platinum: the metal in the catalytic center of a molecular photocatalyst determines the mechanism of the hydrogen production with visible light.** *Angew Chem Int Ed.* 2015; **54**(17): 5044–8.  
[PubMed Abstract](#) | [Publisher Full Text](#)
- Yoshida M, Yomogida T, Mineo T, et al.: **In situ observation of carrier transfer in the Mn-oxide/Nb:SrTiO<sub>3</sub> photoelectrode by X-ray absorption spectroscopy.** *Chem Commun (Camb).* 2013; **49**(71): 7848–7850.  
[PubMed Abstract](#) | [Publisher Full Text](#)
- Minguzzi A, Naldoni A, Lugaresi O, et al.: **Observation of charge transfer cascades in α-Fe<sub>2</sub>O<sub>3</sub>/IrO<sub>2</sub> photoanodes by operando X-ray absorption spectroscopy.** *Phys Chem Chem Phys.* 2017; **19**(8): 5715–5720.  
[PubMed Abstract](#) | [Publisher Full Text](#)
- Braun A, Sivula K, Bora DK, et al.: **Direct Observation of Two Electron Holes in a Hematite Photoanode during Photoelectrochemical Water Splitting.** *J Phys Chem C.* 2012; **116**(32): 16870–16875.  
[Publisher Full Text](#)
- Santomauro FG, Lübcke A, Rittmann J, et al.: **Femtosecond X-ray absorption study of electron localization in photoexcited anatase TiO<sub>2</sub>.** *Sci Rep.* 2015; **5**: 14834.  
[PubMed Abstract](#) | [Publisher Full Text](#) | [Free Full Text](#)
- Achilli E, Minguzzi A, Visibile A, et al.: **3D-printed photo-spectroelectrochemical devices for in situ and in operando X-ray absorption spectroscopy investigation.** *J Synchrotron Rad.* 2016; **23**(2): 622–628.  
[PubMed Abstract](#) | [Publisher Full Text](#)
- Fracchia M, Cristino V, Vertova A, et al.: **Operando X-ray absorption spectroscopy of WO<sub>3</sub> photoanodes.** *Electrochimica Acta.* 2019; **320**: 134561.  
[Publisher Full Text](#)
- Kubli M, Luo L, Bilecka I, et al.: **Microwave-assisted nonaqueous sol-gel deposition of different spinel ferrites and barium titanate perovskite thin films.** *Chimia (Aarau).* 2010; **64**(3): 170–2.  
[PubMed Abstract](#) | [Publisher Full Text](#)
- Zeng G, Shi N, Hess M, et al.: **A General Method of Fabricating Flexible Spinel-Type Oxide/Reduced Graphene Oxide Nanocomposite Aerogels as Advanced Anodes for Lithium-Ion Batteries.** *ACS Nano.* 2015; **9**(4): 4227–4235.  
[PubMed Abstract](#) | [Publisher Full Text](#)
- Grote C, Cheema TA, Garnweitner G: **Comparative Study of Ligand Binding during the Postsynthetic Stabilization of Metal Oxide Nanoparticles.** *Langmuir.* 2012; **28**(40): 14395–14404.  
[PubMed Abstract](#) | [Publisher Full Text](#)
- Erdem D, Shi Y, Heiligtag FJ, et al.: **Liquid-phase deposition of ferroelectrically switchable nanoparticle-based BaTiO<sub>3</sub> films of macroscopically controlled thickness.** *J Mater Chem C.* 2015; **3**(38): 9833–9841.  
[Publisher Full Text](#)
- Jäker P, Koziej D, Detlefs B, et al.: **Dataset for the development of a "Flow cell for operando X-ray photon-in-photon-out studies on photo-electrochemical thin film devices" [Data set].** *Zenodo.* 2022.  
<http://www.doi.org/10.5281/zenodo.6560384>
- <https://imagej.nih.gov/ij/>.
- Schneider CA, Rasband WS, Eliceiri KW: **NIH Image to ImageJ: 25 years of image analysis.** *Nat Methods.* 2012; **9**(7): 671–675.  
[PubMed Abstract](#) | [Publisher Full Text](#) | [Free Full Text](#)
- Momma K, Izumi F: **VESTA 3 for three-dimensional visualization of crystal, volumetric and morphology data.** *J Appl Cryst.* 2011; **44**(6): 1272–1276.  
[Publisher Full Text](#)
- Maslen EN, Streltsov VA, Streltsova NR, et al.: **Synchrotron X-ray study of the**



- electron density in  $\alpha\text{-Fe}_2\text{O}_3$ , *Acta Cryst.* 1994; **50**(4): 435–441.  
[Publisher Full Text](#)
36. Waerenborgh JC, Figueiredo MO, Cabral JMP, *et al.*: **Temperature and Composition Dependence of the Cation Distribution in Synthetic  $\text{ZnFeAl}_{1-z}\text{O}_4$  ( $0 \leq z \leq 1$ ) Spinel.** *J Solid State Chem.* 1994; **111**(2): 300–309.  
[Publisher Full Text](#)
  37. Henke BL, Gullikson EM, Davis JC: **X-Ray Interactions: Photoabsorption, Scattering, Transmission, and Reflection at  $E = 50\text{--}30,000$  eV,  $Z = 1\text{--}92$ .** *At Data Nucl Data Tables.* 1993; **54**(2): 181–342.  
[Publisher Full Text](#)
  38. Shavorskiy A, Ye X, Karslioglu O, *et al.*: **Direct Mapping of Band Positions in Doped and Undoped Hematite during Photoelectrochemical Water Splitting.** *J Phys Chem Lett.* 2017; **8**(22): 5579–5586.  
[PubMed Abstract](#) | [Publisher Full Text](#)
  39. Lee DK, Lee D, Lumley MA, *et al.*: **Progress on ternary oxide-based photoanodes for use in photoelectrochemical cells for solar water splitting.** *Chem Soc Rev.* 2019; **48**(7): 2126–2157.  
[PubMed Abstract](#) | [Publisher Full Text](#)
  40. Zhu X, Guijarro N, Liu Y, *et al.*: **Spinel Structural Disorder Influences Solar-Water-Splitting Performance of  $\text{ZnFe}_2\text{O}_4$  Nanorod Photoanodes.** *Adv Mater.* 2018; 1801612.  
[PubMed Abstract](#) | [Publisher Full Text](#)
  41. Dillert R, Taffa DH, Wark M, *et al.*: **Research Update: Photoelectrochemical water splitting and photocatalytic hydrogen production using ferrites ( $\text{MFe}_2\text{O}_4$ ) under visible light irradiation.** *APL Mater.* 2015; **3**(10): 104001.  
[Publisher Full Text](#)
  42. Reinhard S: **Nanostructured Tungsten Oxide Photoanodes for Photoelectrochemical Hydrogen Production.** Zürich, ETH-Zürich, 2016.  
[Publisher Full Text](#)
  43. Malviya KD, Dotan H, Yoon KR, *et al.*: **Rigorous substrate cleaning process for reproducible thin film hematite ( $\alpha\text{-Fe}_2\text{O}_3$ ) photoanodes.** *J Mater Res.* 2016; **31**(11): 1565–1573.  
[Publisher Full Text](#)
  44. Maabong K, Hu Y, Braun A, *et al.*: **Influence of anodization time on the surface modifications on  $\alpha\text{-Fe}_2\text{O}_3$  photoanode upon anodization.** *J Mater Res.* 2016; **31**(11): 1580–1587.  
[Publisher Full Text](#)
  45. Braun A, Chen Q, Flak D, *et al.*: **Iron Resonant Photoemission Spectroscopy on Anodized Hematite Points to Electron Hole Doping during Anodization.** *ChemPhysChem.* 2012; **13**(12): 2937–2944.  
[PubMed Abstract](#) | [Publisher Full Text](#)
  46. Bard AJ: **Electrochemical methods : fundamentals and applications.** 2nd ed.; New York: Wiley: 2001.  
[Reference Source](#)
  47. Le Formal F, Sivula K, Grätzel M: **The Transient Photocurrent and Photovoltage Behavior of a Hematite Photoanode under Working Conditions and the Influence of Surface Treatments.** *J Phys Chem C.* 2012; **116**(51): 26707–26720.  
[Publisher Full Text](#)
  48. Kenyon CN, Ryba GN, Lewis NS: **Analysis of time-resolved photocurrent transients at semiconductor/liquid interfaces.** *J Phys Chem.* 1993; **97**(49): 12928–12936.  
[Publisher Full Text](#)
  49. Smith SW: **The Scientist and Engineer's Guide to Digital Signal Processing.** 1997.  
[Reference Source](#)
  50. Schroeder DJ: **Astronomical Optics.** 2000.  
[Publisher Full Text](#)
  51. Réfrégier P: **Noise Theory and Application to Physics.** 2004.  
[Publisher Full Text](#)
  52. Knoll GF: **Radiation Detection and Measurement.** Wiley: 2000.  
[Reference Source](#)
  53. Vaseghi SV: **Advanced digital signal processing and noise reduction.** 4th ed. ed.; J. Wiley & Sons: Chichester, U.K, 2008.  
[Publisher Full Text](#)
  54. Chergui M, Collet E: **Photoinduced Structural Dynamics of Molecular Systems Mapped by Time-Resolved X-ray Methods.** *Chem Rev.* 2017; **117**(16): 11025–11065.  
[PubMed Abstract](#) | [Publisher Full Text](#)
  55. Schön D, Xiao J, Golnak R, *et al.*: **Introducing Ionic-Current Detection for X-ray Absorption Spectroscopy in Liquid Cells.** *J Phys Chem Lett.* 2017; **8**(9): 2087–2092.  
[PubMed Abstract](#) | [Publisher Full Text](#)
  56. Schön D, Golnak R, Tesch MF, *et al.*: **Bulk-Sensitive Detection of the Total Ion Yield for X-ray Absorption Spectroscopy in Liquid Cells.** *J Phys Chem Lett.* 2017; **8**(20): 5136–5140.  
[PubMed Abstract](#) | [Publisher Full Text](#)
  57. van Spronsen MA, Zhao X, Jaugstetter M, *et al.*: **Interface Sensitivity in Electron/Ion Yield X-ray Absorption Spectroscopy: The  $\text{TiO}_2\text{--H}_2\text{O}$  Interface.** *J Phys Chem Lett.* 2021; **12**(41): 10212–10217.  
[PubMed Abstract](#) | [Publisher Full Text](#)
  58. Hu TD, Xie YN, Qiao S, *et al.*: **Photoconduction extended x-ray-absorption fine structure of GaAs.** *Phys Rev B.* 1994; **50**(4): 2216–2220.  
[PubMed Abstract](#) | [Publisher Full Text](#)
  59. Vyvenko OF, Buonassisi T, Istratov AA, *et al.*: **X-ray beam induced current—a synchrotron radiation based technique for the *in situ* analysis of recombination properties and chemical nature of metal clusters in silicon.** *J Appl Phys.* 2002; **91**(6): 3614–3617.  
[Publisher Full Text](#)
  60. Buonassisi T, Istratov AA, Pickett MD, *et al.*: **Quantifying the effect of metal-rich precipitates on minority carrier diffusion length in multicrystalline silicon using synchrotron-based spectrally resolved x-ray beam-induced current.** *Appl Phys Lett.* 2005; **87**(4): 044101.  
[Publisher Full Text](#)
  61. Johannes A, Salomon D, Martinez-Criado G, *et al.*: **In operando x-ray imaging of nanoscale devices: Composition, valence, and internal electrical fields.** *Sci Adv.* 2017; **3**(12): eaao4044.  
[PubMed Abstract](#) | [Publisher Full Text](#) | [Free Full Text](#)

# Open Peer Review

Current Peer Review Status:



Version 2

Reviewer Report 13 January 2023

<https://doi.org/10.21956/openreseurope.16671.r30501>

© 2023 Drisdell W. This is an open access peer review report distributed under the terms of the [Creative Commons Attribution License](#), which permits unrestricted use, distribution, and reproduction in any medium, provided the original work is properly cited.



**Walter S. Drisdell** 

Chemical Sciences Division, Lawrence Berkeley National Laboratory, Berkeley, CA, USA

I thank the authors for their detailed reply to my comments, and for the edits to the section discussing data quality for operando spectra collected in the cell. I can now recommend indexing. I also respond to some of the questions from the authors below:

I brought up a parallel electrode configuration because this can be important for systems driven by an externally applied voltage (e.g. applying a voltage with the potentiostat). In that case, if the electrodes are not parallel, there will be a nonuniform electric field at the working electrode which makes it difficult to determine if the X-rays are actually probing the active part of the electrode. In a light-driven system like the one here, I suspect this concern is eliminated, because the electric field at the working electrode is controlled by the illumination. A non-parallel configuration will create a non-uniform electric field at the counter electrode, but that doesn't matter. So for studies of photoelectrochemical systems driven by light, as demonstrated here, this may not be a major concern.

As for mass transport, this can be important for electrochemical reactions in which some of the reactants are solvated species. For example, in electrochemical CO<sub>2</sub> reduction, dissolved CO<sub>2</sub> is a reactant, and is present at low concentration due to its small Henry coefficient. In that case, it's easy to deplete the dissolved CO<sub>2</sub> under operation, unless there is sufficient mass transport (usually via liquid flow) to replenish CO<sub>2</sub> at the electrode surface. The cell design shown here would be sub-optimal for such a reaction due to (I presume) low flow rates and low mass transport. Also, many electrochemical reactions (including CO<sub>2</sub> reduction) form gas-phase products as bubbles on the electrode surface, which can interfere with measurements if they cannot be swept away through liquid flow. The cell reported in this paper may not be ideal for such reactions, given (I presume) a low liquid flow rate due to the small flow channels. But for other reactions, this will not be a concern. So it depends on the application.

Lastly, I thank the authors for elaborating on the reasoning for two small silicon nitride windows instead of one larger one. The in situ cells I have used featured single, larger silicon nitride windows, but we were not particularly concerned about water pressure. I wonder if the pressure

in this cell might be higher due to the microfluidic liquid flow? Regardless, I appreciate the authors elaborating on the engineering decisions for this.

**Competing Interests:** No competing interests were disclosed.

**Reviewer Expertise:** In situ synchrotron X-ray characterization, chemistry, electrocatalysis, energy materials.

**I confirm that I have read this submission and believe that I have an appropriate level of expertise to confirm that it is of an acceptable scientific standard.**

Reviewer Report 11 January 2023

<https://doi.org/10.21956/openreseurope.16671.r30500>

© 2023 Minguzzi A. This is an open access peer review report distributed under the terms of the [Creative Commons Attribution License](#), which permits unrestricted use, distribution, and reproduction in any medium, provided the original work is properly cited.



**Alessandro Minguzzi** 

Dipartimento di Chimica, Università degli Studi di Milano, Milan, Italy

Dear Philipp Jäker,

I acknowledge and appreciate your reply to my review of your interesting paper.

I think that your responses are fully satisfactory, and I have no other comments. In my opinion the paper can be considered at the end of its editorial path.

For what concerns current cell versions, your conclusions based on our papers are substantially correct. In the latest version of our cell, the electrode is as close as possible to the mylar film to minimize the absorption from the solution. At the same time, a too thin layer of solution leads to not-negligible ohmic drops. It is unfortunately impossible for us to precisely determine the thickness of the solution (estimated in the range 100-300 microns), but this setup allowed us to successfully work at the Ni-K edge (Malara *et al.*, 2020<sup>1</sup> and Tsyganok *et al.*, 2020<sup>2</sup>).

If the studied reaction involves gas formation, the insulation of part of the sample area due to bubble retention is another factor to consider when a quite thin solution layer is desired. In this sense, your cell has undoubtedly the main advantage of guaranteeing an efficient bubble removal by a correct design of the solution flux.

## References

1. Malara F, Fracchia M, Kmentová H, Psaro R, et al.: Direct Observation of Photoinduced Higher Oxidation States at a Semiconductor/Electrocatalyst Junction. *ACS Catalysis*. 2020; **10** (18): 10476-10487 [Publisher Full Text](#)
2. Tsyganok A, Ghigna P, Minguzzi A, Naldoni A, et al.: Operando X-ray Absorption Spectroscopy (XAS) Observation of Photoinduced Oxidation in FeNi (Oxy)hydroxide Overlayers on Hematite ( $\alpha$ -Fe<sub>2</sub>O<sub>3</sub>) Photoanodes for Solar Water Splitting. *Langmuir*. 2020; **36** (39): 11564-11572 [PubMed](#)

[Abstract](#) | [Publisher Full Text](#)

**Competing Interests:** No competing interests were disclosed.

**Reviewer Expertise:** electrochemistry, photoelectrochemistry, X-ray spectroscopies

**I confirm that I have read this submission and believe that I have an appropriate level of expertise to confirm that it is of an acceptable scientific standard.**

---

**Version 1**

Reviewer Report 14 November 2022

<https://doi.org/10.21956/openreseurope.15578.r30353>

© 2022 Drisdell W. This is an open access peer review report distributed under the terms of the [Creative Commons Attribution License](#), which permits unrestricted use, distribution, and reproduction in any medium, provided the original work is properly cited.



**Walter S. Drisdell** 

Chemical Sciences Division, Lawrence Berkeley National Laboratory, Berkeley, CA, USA

The authors demonstrate a cell design for in situ X-ray absorption spectroscopy (XAS), particularly in high energy resolution fluorescence detection (HERFD) mode, on aqueous photoelectrochemical systems. The design emphasizes the ease of changing samples, so robust comparisons can be made between different catalysts within a single block of beamtime at a synchrotron facility. The design also specifically emphasizes solar light as a driver for the chemistry. Most in situ cells for XAS operate in the dark using externally applied voltages as the driver. Recent interest in direct photo-driven systems means a cell that accommodates solar light is desirable.

The cell design and operation are demonstrated thoroughly, but there are clear downsides that come with the "quick swap" sample scheme. Generally speaking, electrochemical cells for in situ XAS must either bring the X-rays in through the back of the sample, or through the electrolyte before impinging on the front of the sample. This design does the latter, because this means samples are not directly deposited onto the expensive (and fragile) silicon nitride windows, and can therefore be swapped more easily. But even the thin (400 - 500 micron) liquid layer between the window and the sample introduces significant loss of signal, a roughly 70% loss compared to the ex situ measurement. This loss will get worse for any application looking at lighter metals as well. The authors demonstrate Fe K-edge data, but Cr K-edge or Ti K-edge would have worse signal loss.

In addition, the thin liquid channels place constraints on the electrochemistry; for example, the counter electrode is not parallel to the working electrode sample, instead located within one of the sub-mm flow channels past the main cell volume. The cell also lacks a membrane, so Pt from the counter electrode could migrate to the sample surface (although the fact that the counter electrode is so far away may help with this). I suspect that there may be upper limits on mass



transport as well, although these did not come into play in the demonstrations shown here, and are likely less important for light-driven systems than those run via external voltage. If the sample were deposited on the window instead, and the X-rays and solar light were brought in through the back, there would be no constraints on the liquid side of the cell, enabling a parallel electrode configuration and larger flow channels that can support high current densities. Also, there would be minimal attenuation of the X-ray signal by the electrolyte, since the electrolyte is on the far side of the sample.

As I see it, the advantages to this cell are the ability to easily change samples, and that samples need not be partially transparent to X-rays or solar light (in other words, samples need not be thin films, although it's unclear if thicker samples can be mounted or if the size limitations effectively mean that thin films must be used). For some applications, for example screening large numbers of potential photocatalyst materials, this is a big advantage and this cell design will be useful. For other studies, using a "sample on window" design may be better because it gives better XAS signal and can support higher current density operation, even though sample preparation and swapping is more difficult.

I do have one question about the design: I do not understand why two silicon nitride windows are used. Is there a separate window for input X-rays vs. detected fluorescence? Figure 5 suggests not. Is one window for the solar light while the other is for X-rays? It seems to me that a single window with larger area would work better, as is shown schematically in Figure 1. This is especially true given that Figure 5 shows that not all of the fluorescence can be extracted because the window is not large enough to cover the full solid angle. The discussion of this figure is confusing, in fact, because it mentions overlap between photon-in and photon-out beams, but in reality fluorescence is generated only where the input photons impinge upon the sample and can be detected as long as they can pass through the window at 90 degrees relative to the input beam. There is no "output beam" that matches the profile shown in Figure 5, that seems to more accurately describe which parts of the sample can be "seen" by the detector. Ideally, the detector should be able to "see" the entire illuminated area on the sample, but from this Figure it seems that is not the case in this design.

A final minor correction: in the plain text summary, the phrase "within a signal device" should read "within a single device".

**Is the rationale for developing the new method (or application) clearly explained?**

Yes

**Is the description of the method technically sound?**

Yes

**Are sufficient details provided to allow replication of the method development and its use by others?**

Yes

**If any results are presented, are all the source data underlying the results available to ensure full reproducibility?**

Yes

**Are the conclusions about the method and its performance adequately supported by the findings presented in the article?**

Yes

**Competing Interests:** No competing interests were disclosed.

**Reviewer Expertise:** In situ synchrotron X-ray characterization, chemistry, electrocatalysis, energy materials.

**I confirm that I have read this submission and believe that I have an appropriate level of expertise to confirm that it is of an acceptable scientific standard, however I have significant reservations, as outlined above.**

Author Response 30 Nov 2022

**Philipp Jäker**, ETH Zürich, Zurich, Switzerland

Dear Walter S. Drisdell,

We highly appreciate your encouraging and constructive report and generally agree with your comprehensive summary about the advantages and disadvantages of design considerations concerning the position of the thin film sample, e.g. front vs back with respect to incident X-ray beam direction. I don't quite understand the potential issue with the non-parallel placement of working and counter electrode. Mass transport limitations near the very small Pt wire could indeed be an issue but I would argue that the Pt surface area can still substantially and relatively easily be enhanced. At low to moderate mass transport limitations, the potentiostat is still able to compensate by increasing the counter electrode's bias. Potentially more significant than mass transport is the uncompensated resistance of the working-reference-electrode circuit branch. On a rough back on the envelope calculation modelling the liquid channels as resistance elements might add about 100 mV to the working electrode to what currently is measured with respect to the reference electrode. It is very briefly mentioned following figure 3 that uncompensated resistance should be analyzed in future work. I agree that a membrane could provide protection against cross-electrode contamination both from the electrode material itself as well as from the water splitting reaction products. Hopefully, others will improve this cell design and further quantify some of its measurement properties. Regarding potential sample thickness and type: If one exactly reproduces this cell one will be constrained by the working electrodes (WE) (here FTO), width and length but not thickness to some extent. The working electrode slot within the cell currently is thicker than the FTO and so leaves room in the  $\mu\text{m}$  to mm range for thicker films. The liquid channel thickness is completely predefined within the  $\text{Si}/\text{Si}_3\text{N}_4$  chip. The cell crucially relies upon a very smooth working electrode surface sealing the channel within the  $\text{Si}/\text{Si}_3\text{N}_4$ . If this is achieved one can also use different electrode materials as long as the principle width and length dimensions are considered. One can imagine using a smooth metallic electrode as back-side transparency is not relevant. Or use a metallic electrode to study photoelectrochemical processes within an X-ray absorbing electrolyte. Regarding one vs two  $\text{Si}_3\text{N}_4$ :

I agree that one larger  $\text{Si}_3\text{N}_4$  window would render the experiment potentially simpler and increase signal detection. However, Norcada, the company responsible for design and manufacturing, recommended this window size as any further increase only increases the mechanic instability against the water pressure. I cannot provide you with anything more concrete or even quantitative. As Norcada improves their production process they might be able to produce larger windows with the same thickness but greater mechanical stability. Regarding the discussion of Figure 5: I agree that the discussion was a bit confusing and I thank you for your input especially regarding what we described as “photon-out” beam. Indeed, a more appropriate description than that is actually the Bragg crystal analyzer focus on the sample. I have now rewritten large parts of that section and hope it to be more understandable. But the previous conclusion remains in that there is an underlying mismatch between the spectrometer focus and the X-ray excited area. Small X-ray beam sizes, thinner electrolyte thicknesses or larger  $\text{Si}_3\text{N}_4$  windows may even fully reduce it but all come with different disadvantages/consequences.

**Competing Interests:** No competing interests were disclosed.

Reviewer Report 29 June 2022

<https://doi.org/10.21956/openreseurope.15578.r29519>

© 2022 Minguzzi A. This is an open access peer review report distributed under the terms of the [Creative Commons Attribution License](#), which permits unrestricted use, distribution, and reproduction in any medium, provided the original work is properly cited.



**Alessandro Minguzzi**

Dipartimento di Chimica, Università degli Studi di Milano, Milan, Italy

This is a valuable contribution that will be of high interest for synchrotron users and experts in photoelectrochemistry (in-situ/operando) XAS. I think it can be indexed as it is provided that the following comments are considered by the authors.

1. The sentence in the Introduction, “Current cell versions are limited by electrochemical noise or unnecessarily high X-ray beam attenuation.” can be improved, since previous works (for example Fracchia *et al.*, 2019<sup>1</sup>) clearly show the effectiveness of other XAS cells for in-situ/operando experiments in photoelectrochemistry with no significant noise or X-ray attenuation.
2. For what concerns the total ion yield, I suggest a deeper discussion. Indeed, this ion current flow is the result of electrons ejected after X-rays hit the sample. Being the photoelectrode under a bias, the loss of these electrons is (or might be) compensated by electrons circulating in the external circuit (indeed, Fig. 6 reports an electric current) that are accompanied by ionic flowing in the electrolyte solution.

This (photo)current is therefore both electronic and ionic, this is why I find that the term TIY is possibly not fully appropriate. However, I do agree that monitoring this signal might

represent a very interesting new source of information! Moreover, the recording of this signal is possible thanks to the electrolyte fluxing that represents a significant added-value of this cell. In other conditions (such as bubble formation), the noise in the current signal won't allow it. This aspect of course relates to point 1 of this review.

3. Interesting reviews have appeared on the topic and I think it might be worth citing them (for example: Deng *et al.*, 2020<sup>2</sup>).

4. Fig. 6 has no numbers at the x-axis, but the reader should be allowed to have an idea of the time scale of these experiments.

### References

1. Fracchia M, Cristino V, Vertova A, Rondinini S, et al.: Operando X-ray absorption spectroscopy of WO<sub>3</sub> photoanodes. *Electrochimica Acta*. 2019; **320**. [Publisher Full Text](#)
2. Deng J, Zhang Q, Lv X, Zhang D, et al.: Understanding Photoelectrochemical Water Oxidation with X-ray Absorption Spectroscopy. *ACS Energy Letters*. 2020; **5** (3): 975-993 [Publisher Full Text](#)

**Is the rationale for developing the new method (or application) clearly explained?**

Yes

**Is the description of the method technically sound?**

Yes

**Are sufficient details provided to allow replication of the method development and its use by others?**

Yes

**If any results are presented, are all the source data underlying the results available to ensure full reproducibility?**

Yes

**Are the conclusions about the method and its performance adequately supported by the findings presented in the article?**

Yes

**Competing Interests:** No competing interests were disclosed.

**Reviewer Expertise:** electrochemistry, photoelectrochemistry, X-ray spectroscopies

**I confirm that I have read this submission and believe that I have an appropriate level of expertise to confirm that it is of an acceptable scientific standard, however I have significant reservations, as outlined above.**

Author Response 30 Nov 2022



**Philipp Jäker**, ETH Zürich, Zurich, Switzerland

Dear Alessandro Minguzzi,

We highly appreciate your encouraging and constructive report and would like to respond to the four comments you recommended us to consider.

1. We removed our claim that current cell versions are limited by electrochemical noise based on the following arguments/reasons
  1. Most publications do not provide adequate data/figures to quantitatively assess the signal-to-noise ratio (S/N) in electrochemical measurements, e.g. recordings of voltage or current. My claim was based on Figure S5 of Yoshida et al.<sup>1</sup> publication which lacks real physical units and an actual scale along the y-axis.
  2. We ourselves do not address the electrochemical S/N in the same manner we did to assess the S/N of the HERFD-XAS measurements although we claimed to do so. It only remains a qualitative, visual inspection of respective current and voltage measurements, which I do regard as insufficient given the S/N is a well-defined quantitative property. This would mean falling short regarding once own standards.
  3. However, a cell's X-ray beam attenuation on the basis of well-established Lambert-Beer like exponential attenuation laws can be compared quite thoroughly once the energy range, absorption coefficient and material thickness are known for example using this web based application relying on tabulated values: [https://henke.lbl.gov/optical\\_constants/](https://henke.lbl.gov/optical_constants/).

In our cell design the X-ray beam has to pass 500 nm of Si<sub>3</sub>N<sub>4</sub> and 500 µm of approximately pure water, disregarding the minor acidic or basic electrolyte ion contribution.

Please correct me if mistaken: Your 3D-printed cells described in your publication<sup>2</sup> I referenced were designed with a 100 µm Mylar or polyacrylic resin window followed by a 1 mm thick electrolyte layer which the X-ray beam had to pass.

The cell you referenced in your report<sup>3</sup> features a 10 µm Mylar window and an unclear electrolyte thickness, as you only provide two spatial dimensions ("2 x 2 mm<sup>2</sup>"). Does one of those spatial dimensions describe the thickness along the X-ray beam axis, perpendicular to your working electrode surface and as such the electrolyte thickness? Although, Si<sub>3</sub>N<sub>4</sub> is about 2-3 times denser than the polymers you used the 20-200 times greater thickness is the defining parameter. In combination with at least a 2 times thicker electrolyte layer, the X-ray attenuation of our cell compared to your cells is significantly reduced.

Additionally, your studies report XAS measurements at the L<sub>III</sub> edges of W and Ir, slightly above 10 keV where attenuation becomes less severe as the energy dependent absorption coefficients generally decrease with increasing energy.

Thus, I believe that "current cell versions often do not minimize X-ray beam attenuation" is

an objectively fair statement to make based on combined empirical & modelled evidence.

1. I agree that we could have been more critical about the potential promises about X-ray absorption measurements via ionic current detection. Therefore relevant text passages have been altered and a crucial recent publication has been referenced. The work of van Spronsen et al.<sup>4</sup> illustrates how critical a deep understanding of electrical/electrochemical measurements is in order to decipher the current contributions upon X-ray absorption. That is why we have not drawn any conclusions from our measured current other than that it clearly shows that X-ray beam induced currents can be measured and that the current trace resembles X-ray absorption Fe K-edge spectra measured *via* HERFD-XAS. However, I remain very optimistic that carefully analyzing this cell type's measurement properties and possibly redesigning the cell might enable experiments to reveal more details about X-ray beam induced currents and what information they can provide.

1. I appreciate your literature suggestions but without a clear statement which claims in our manuscript currently are not supported I refrain from citing it. I am aware of your suggested publication and I do not see crucially relevant information given they that has not already been covered in quite a number of recent reviews, even if the considered one focuses specifically on operando X-ray absorption spectroscopy in photoelectrochemical systems. Additionally, in my view one should be careful in citing review articles instead of the relevant primary literature as this obscures a clear reference literature path and might even be used for gaming bibliometrics.

2. The HERFD-XAS scan duration was reported as 60 s in our experimental section. But agree that it is easier to read with appropriate axis labels and therefore added them to the figure, as well as the X-ray on/off duration in the inset.

1. Yoshida, M.; Yomogida, T.; Mineo, T.; Nitta, K.; Kato, K.; Masuda, T.; Nitani, H.; Abe, H.; Takakusagi, S.; Uruga, T.; Asakura, K.; Uosaki, K.; Kondoh, H., In situ observation of carrier transfer in the Mn-oxide/Nb:SrTiO<sub>3</sub> photoelectrode by X-ray absorption spectroscopy. *Chem. Commun.* **2013**, 49, (71), 7848-7850.

2. Achilli, E.; Minguzzi, A.; Visibile, A.; Locatelli, C.; Vertova, A.; Naldoni, A.; Rondinini, S.; Auricchio, F.; Marconi, S.; Fracchia, M.; Ghigna, P., 3D-printed photo-spectroelectrochemical devices for in situ and in operando X-ray absorption spectroscopy investigation. *J. Synchrotron Rad.* **2016**, 23, (2), 622-628.

3. Fracchia, M.; Cristino, V.; Vertova, A.; Rondinini, S.; Caramori, S.; Ghigna, P.; Minguzzi, A., Operando X-ray absorption spectroscopy of WO<sub>3</sub> photoanodes. *Electrochimica Acta* **2019**, 320, 134561.

4. van Spronsen, M. A.; Zhao, X.; Jaugstetter, M.; Escudero, C.; Duchoň, T.; Hunt, A.; Waluyo, I.; Yang, P.; Tschulik, K.; Salmeron, M. B., Interface Sensitivity in Electron/Ion Yield X-ray Absorption Spectroscopy: The TiO<sub>2</sub>-H<sub>2</sub>O Interface. *J. Phys. Chem. Lett* **2021**, 12, (41), 10212-10217.

**Competing Interests:** No competing interests were disclosed.